AGU PUBLICATIONS

JGR

Journal of Geophysical Research: Planets

BRIEF REPORT

10.1002/2013JE004526

Key Points:
- Bands offset older features through expansion and strike-parallel motion
- Double ridges preserve strike-parallel motion, and contraction or expansion
- Some of the strain recorded by bands can be accommodated by double ridges

Supporting Information:
- Readme
- Figure S1
- Figure S2
- Figure S3
- Figure S4
- Figure S5
- Figure S6
- Figure S7
- Figure S8
- Figure S9
- Figure S10
- Figure S11
- Figure S12
- Figure S13
- Figure S14

Correspondence to:
C. Culha,
c.culha4@berkeley.edu

Citation:
Culha, C., A. G. Hayes, M. Manga, and A. M. Thomas (2014), Double ridges on Europa accommodate some of the missing surface contraction, *J. Geophys. Res. Planets*, *119*, doi:10.1002/2013JE004526.

Received 12 SEP 2013
Accepted 29 JAN 2014
Accepted article online 4 FEB 2014

Double ridges on Europa accommodate some of the missing surface contraction

Cansu Culha[1], Alexander G. Hayes[2], Michael Manga[1], and Amanda M. Thomas[3]

[1]Department of Earth and Planetary Science, University of California, Berkeley, California, USA, [2]Department of Astronomy, Cornell University, Ithaca, New York, USA, [3]Department of Geophysics, Stanford University, Stanford, California, USA

Abstract Crosscutting relationships of tectonic lineaments on Europa record the history of surface deformation. We mapped the displacement and orientation of older features crosscut by two types of lineaments: bands and double ridges. These measurements allow us to determine both the strike-perpendicular and strike-parallel displacement along investigated features. Double ridges record both ridge-perpendicular contraction and expansion, with a mean of 0.16 ± 0.06 km (needs space) of contraction based on the analysis of 16 double ridges. Bands record expansion, with a mean of 3.33 ± 0.27 km for the six bands analyzed, but with perpendicular displacement less than their apparent morphologic widths of 3–24 km. The implied global surface strain for double ridges (including those that expand) and bands is 2.22 ± 0.76% contraction and 7.60 ± 3.7% expansion, respectively. Double ridges thus may accommodate part of the surface expansion recorded by bands. Most current models for double ridges do not predict contraction. The models that satisfy the observations for bands are "slow-spreading" models, cryovolcanism, and folding.

1. Introduction

Jupiter's moon Europa is covered by overlapping linear features that are longer and more uniform along strike as compared to tectonic features on Earth. Because they are numerous and extend over great distances, they provide an opportunity to study the history of surface deformation over large spatial scales [*Schenk and McKinnon*, 1989; *Sullivan et al*., 1998; *Nimmo and Gaidos*, 2002].

The two most abundant types of lineaments on Europa are bands (Figure 1b) and double ridges (Figures 1c and 1d). Double ridges consist of two parallel ridges and are ubiquitous on Europa's surface. The along strike-perpendicular width of double ridges ranges from 0.2 to 4 km, but individual ridge widths vary only slightly. They can also be hundreds of kilometers long [*Greeley et al*., 2000]. Bands typically possess a medial valley and, in most cases, express a morphologic symmetry about this valley that has some similarity to the mid-ocean ridges produced by seafloor spreading on Earth [*Sullivan et al*., 1998; *Prockter et al*., 2002; *Nimmo et al*., 2003; *Kattenhorn and Hurford*, 2009; *Prockter and Patterson*, 2009]. Bands are widely accepted to be lineaments that form through dilation [*Schenk and McKinnon*, 1989; *Pappalardo and Sullivan*, 1996; *Sullivan et al*., 1998; *Tufts et al*., 2000], but they also show evidence of lateral motion, leading to oblique opening along lineaments [*Tufts et al*., 2000; *Prockter et al*., 2002]. Bands are typically less than 30 km wide [*Schenk and McKinnon*, 1989; *Pappalardo and Sullivan*, 1996] and may be responsible for generating a large fraction of Europa's exposed surface [*Prockter et al*., 2002].

A variety of models have been proposed to create lineaments on Europa, including diapirism [*Head and Pappalardo*, 1999], processes analogous to spreading at Earth's mid-ocean ridges to make bands [*Prockter et al*., 2002], folding of ductile ice to make both bands and ridges [*Manga and Sinton*, 2004], shearing to make ridges by heating and thermal expansion of ice [*Nimmo and Gaidos*, 2002], opening-mode fractures [*Greenberg et al*., 1998], cryovolcanism [*Kadel et al*., 1998], rotating plates to form both bands and ridges [*Hoppa et al*., 1999], and shearing of opening-mode fractures [*Aydin*, 2006]. Each of these models predicts different lineament-perpendicular displacements, permitting an observational test that can discriminate among many of these models.

Here we use Galileo solid-state imaging (SSI) images to map the displacements along lineaments. We exploit crosscutting relationships to map and calculate both strike-parallel (strike-slip) and strike-perpendicular displacements. We use these observations to evaluate conceptual models for ridge and band formation. We confirm that this technique can identify expansion along bands [*Schenk and McKinnon*, 1989; *Pappalardo and Sullivan*, 1996; *Sullivan et al*., 1998; *Tufts et al*., 2000] but also find double ridges that record net contraction.

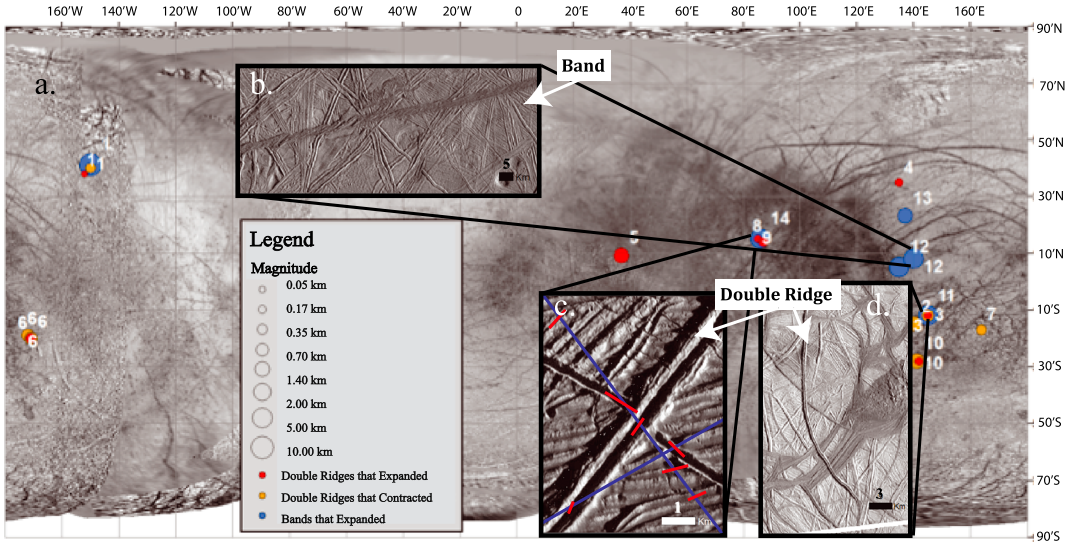

Figure 1. (a) Map of Europa summarizing results. The size of the circles is proportional to the magnitude of the strike-perpendicular displacement. The colors indicate type of feature analyzed. The numbers correspond to regions in Tables 1 and 2. (b–d) Examples of bands and double ridges. Figure 1b corresponds to the mapped band in region 12 and further analyzed in Figure 4. Figure 1c corresponds to the mapped double ridge in region 8 (further analyzed in Figure 3), and it is an illustration of the method for calculating the spacing of lineaments. The line drawn from left top corner to bottom right is 10.4 km long and intersects six double ridges. The other line is 6.4 km long and intersects two double ridges. We repeat this procedure for multiple images and tally the length of the lines and number of crossing features. Since some of the images are better than others, we give more weight to those with higher resolution. Figure 1d indicates to the mapped double ridge in region 2, further analyzed in Figure 4.

2. Methods

In order to identify displacements along lineaments we identify and map older crossing features that are displaced along the younger lineament, designated hereafter as the "main lineament." If motion along the main lineament involves only strike-parallel displacement, then all (older) crosscutting features will have the same observed offset. If, however, there is displacement perpendicular to the main lineament, the along-strike offset (total offset) will depend on the angle of incidence, θ_i, between the main lineament and the i^{th} older lineament that is intersected. We illustrate this effect in Figure 2. As the angle of incidence increases, the amount of

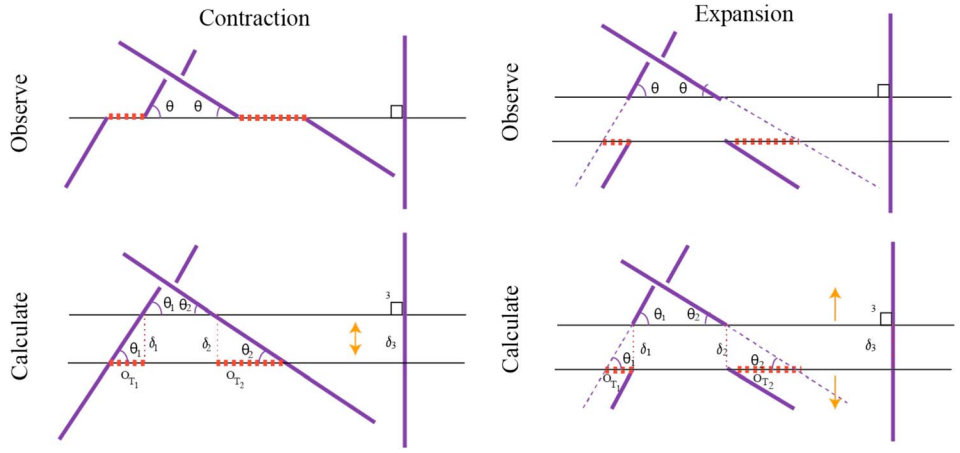

Figure 2. From two observable parameters, angle and offset, we can calculate the amount of displacement parallel and perpendicular to the main lineament. (left column) Contraction without strike-parallel motion (90° angle shows no offset) and (right column) expansion without strike-parallel motion. The strike-parallel motion would either add to, or subtract from, the amount of observed offset. Positive δ defines expansion. Negative δ means contraction. Observed right-lateral offset is positive, and left lateral is negative.

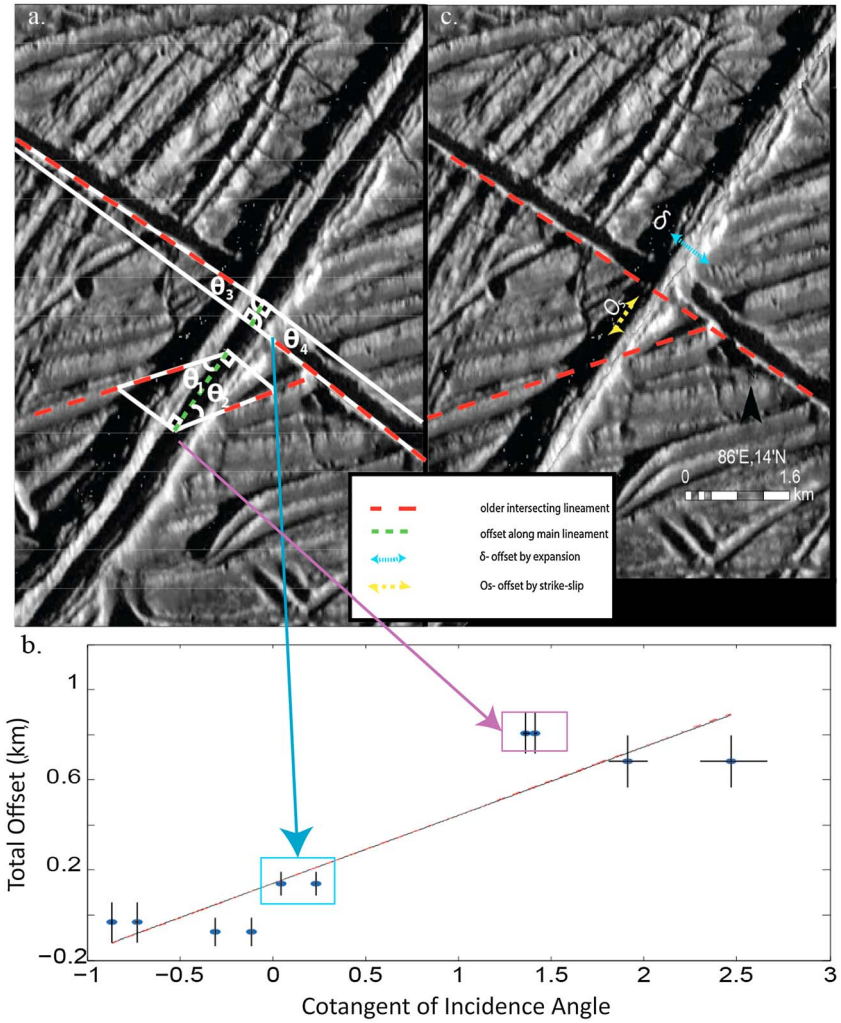

Figure 3. (a) An example of a crosscutting feature on Europa (region 8, see Figure 1). Each side of the crosscut feature is analyzed separately. The angle (θ) is the angle between the main lineament and the older lineament. Each of the offset displacements, marked by the dashed green line in Figure 3a, is compared to the incidence angle. (b) Compares the cotangent of the incidence angle and the total offset in kilometers of the intersected lineament pairs; the *y* intercept gives the total offset by strike slip (O_s) and the slope is the expansion (δ). (c) Reconstructs the plates after removing the strike-parallel motion and expansion based on the fit in Figure 3b. This example is an ideal region to explain some of the mapping criteria. The older feature intersected at a smaller incidence angle contains multiple sublineaments. In certain features we may average multiple parts of a crosscut feature. In this case, we mapped the pair that fit our criteria. The other pairs (1) crosscut another older lineament under the main lineament and (2) cannot be clearly connected, but the pair we do map have similar shadow patterns, have similar appearance, and are crosscut by unusually oriented ridges on their southern side. By mapping multiple crossed features, we account for possible incorrect pairs.

apparent horizontal displacement decreases; older lineaments that are perpendicular to the main lineament have no offset due to expansion or contraction.

On geometric grounds, assuming uniform displacement along the lineament, we expect

$$O_{T_i} = O_S + \delta \cot(\theta_i) \quad (1)$$

where O_{T_i} is the total (measured) offset, O_S is the strike-parallel offset, and δ is the lineament perpendicular expansion or contraction, illustrated in Figure 2. When making measurements we record two angles for each intersection (the angles on either side of the main lineament are not necessarily identical, but the total offset is the same), as shown in Figure 3. The component of the perpendicular displacement (δ) is positive if the lineament has expanded and negative if it has contracted. By observing multiple intersections, we can fit measurements of

apparent along-strike offset and cotangent of the incidence angle to determine the true mean strike-parallel and perpendicular displacements along the main lineament. We note that the approach we adopt here to identify strike-parallel displacements is relevant for assessing polar wander models [*Sarid et al*., 2002; *Rhoden et al*., 2012] in addition to revealing whether individual lineaments experience expansion or contraction.

Coulter [2009] independently performed a conceptually similar study. Our approach differs in how we fit models to the measurements. First, our geometrical analysis of the features allows us to fit linear models and quantify uncertainties about the data we interpret. Second, it naturally incorporates the "intersection of two crosscutting features" technique suggested by *Coulter* [2009]. Third, when mapping the two older features that intersect, we do not map the ones that overlap beneath the lineament of interest, because we cannot identify the amount of deformation that the middle lineament caused on the oldest. In addition, we cannot tell the difference in ages of the three lineaments. Therefore, mapping these features would give skewed results; hence, we do not include them in the present study. Fourth, we assume that if a younger feature crosses the lineament of interest, it will not alter the prior history recorded by crosscutting relationships. We exclude features that do not have three or more crosscutting features, have poor resolution, have been altered to a point that they are not continuous, or cannot be clearly identified as either a double ridge or a band.

The nonplanar maps were created using ArcGIS. Examples of mapped features are provided in the figures. The mapped lineaments were chosen based on the number of features each of the bands or double ridges cross, the continuity and visibility of the lineaments, consistency with the descriptions of double ridges or bands, and the coverage and resolution of the SSI images. The small number of features that we do study (relative to the number of features that are visible on Europa) is due to the combination of several limitations. Galileo imaged only 10% of the surface at better than 200 m/pixel [*Greeley et al*., 2000]. Furthermore, Galileo SSI obtained only two swaths at high resolution ($<$200 m/pixel), causing our analysis to be clustered along these two strips (Figure 1). Additionally, wider bands increase the chance of other features forming on top of the lineament and older features crosscutting each other beneath the band, complicating our analysis (e.g., Thynia Linea). A wide lineament also increases the error in projecting crosscut features to the center of the main lineament (see the errors in Table 2), failing the criteria described above. The analyzed bands are not wider than ~25 km. Finally, only some of the ridges and bands within these images had greater than or equal to three identifiable and older crosscut features. One of our main challenges is identifying the offsets along these features given the poor resolution. Some of the lineaments preserve enough offset to overcome the limitations induced by low resolution, and some do not. We account for these limitations in our interpretational error analysis. We also note that this study can be expanded if and when additional high-resolution views of Europa's surface become available.

The uncertainty in our statistical inferences, such as our interpretational errors and observational errors associated with matching lineament pairs, is calculated using a Gibbs sampling algorithm [*Smith and Robert*, 1993], a type of Markov chain, to randomize each mapped point within a radius of two resolution cells. We report the errors through the standard deviation of the distributions generated by Markov chain Monte Carlo simulations at the 68% confidence interval (1 standard deviation). The goal is to quantify how random errors in the mapping affect the measured angles and distances, altering the final results. Within each simulation, mapped points are displaced in random directions by distances determined by random sampling of a Gaussian distribution centered about zero with a standard deviation equal to two resolution cells of the respective SSI images.

In addition to interpretational error, our analysis includes several implicit assumptions. First, the older lineament will remain linear as it intersects the main lineament. Second, no movement along crosscutting features took place after the formation of the main lineament. Third, although *Patterson et al*. [2006] provide examples of nonrigid plates on Europa, motion on either side of the lineament over short distances is assumed to be spatially homogeneous (i.e., motion can be modeled using rigid plates). Fourth, although *Nimmo and Schenk* [2006] report a few features that preserved several hundreds of meters of vertical thrust, we assume that vertical motions have a very small impact on the amount of strike-perpendicular motion that is preserved. If data do not fall on a straight line within uncertainty of our measurements, then this is likely the result of a violation of one or more of the above assumptions. It is also important to note that we assume the lost and gained materials are added or subtracted along the center of the lineament.

Table 1. Summary of Mapped Double Ridges[a]

Region	Latitude	Longitude	Number of Intersecting Lineaments	Expansion δ (km)	Strike-Parallel O_s (km)	χ^2	Resolution (m/pixel)
1.3	40	−150	8	−0.28 ± 0.18	−0.09 ± 0.11	0.42	169.37
2	−15	140	14	−1.19 ± 0.15	2.08 ± 0.08	1.59	222.60
3.1	−12	145	11	0.15 ± 0.25	1.00 ± 0.13	1.12	223.06
3.2	−12	145	3	−0.70 ± 0.36	1.38 ± 0.12	0.36	223.06
1.2	38	−152	6	0.05 ± 0.30	−0.84 ± 0.23	0.82	169.37
4	35	135	12	0.17 ± 0.07	0.06 ± 0.05	2.29	63.03
5	9	37	9	1.09 ± 0.18	−0.45 ± 0.08	0.28	104.65
6.3	−19	−172	7	−0.64 ± 0.40	0.35 ± 0.12	0.23	230.05
6.4	−19	−172	7	−0.04 ± 0.29	−0.82 ± 0.15	1.43	230.05
6.2	−20	−171	3	−0.45 ± 0.26	0.13 ± 0.29	0.31	230.05
6.1	−20	−171	11	0.35 ± 0.21	0.11 ± 0.13	0.35	230.05
7	−17	164	8	−0.26 ± 0.10	1.53 ± 0.03	2.00	49.60
8	14	87	5	0.30 ± 0.03	0.14 ± 0.03	1.65	20.60
9	15	85	3	0.17 ± 0.05	0.55 ± 0.04	6.16	20.60
10.1	−28	141	3	−1.40 ± 0.11	1.01 ± 0.05	5.41	54.75
10.2	−28	142	5	0.11 ± 0.15	0.31 ± 0.07	2.24	54.75

[a]The region number corresponds to numbers on the figures. The latitudes and longitudes are with respect to the equator and the prime meridian. Negative δ indicates contraction, and positive indicates expansion. Negative strike-parallel displacement is left-lateral motion, and positive strike-parallel displacement is right-lateral motion. Goodness of fit is reduced chi-square, χ^2. The stated uncertainties are one sigma (68% confidence interval) derived using Markov chain Monte Carlo simulation with a radius of two resolution cells.

3. Results

Tables 1 and 2 summarize the mapped lineaments and the inferred strike-parallel and strike-perpendicular (δ) displacements. We observe a correlation between lineament morphology and displacement: bands typically record divergence while some double ridges preserve convergence and have smaller strike-parallel displacement than bands. The location and magnitude of strike-perpendicular displacement are mapped in Figure 1. Both double ridges and bands show right- and left-lateral motion.

Next we consider one example of each of these features in detail to illustrate the results of mapping and the agreement between the model (equation (1)) and the measurements; these two examples are shown in Figure 4. The supporting information also contains analogous maps and figures for all the studied lineaments.

3.1. Double Ridges

Figure 4a shows a right-lateral offset double ridge. Variation of offset with incidence angle, however, indicates that there is lineament-perpendicular contraction as well as strike-parallel displacement, in this case $\delta = -1.19 \pm 0.15$ km and $O_S = 2.08 \pm 0.08$ km.

Of the 16 mapped double ridges, seven show contraction (between 0.28 ± 0.18 and 1.40 ± 0.11 km) and five show expansion (between 0.17 ± 0.05 and 1.09 ± 0.18 km). The crosscutting features with high incidence angle show that there is also a strike-parallel component of displacement between -0.82 ± 0.15 km (left lateral) and 2.08 ± 0.08 km (right lateral) for contracted double ridges. We note, however, that only one contracted feature records (within error) left-lateral strike-parallel displacement. For expanded double ridges,

Table 2. Summary of Mapped Bands[a]

Region	Latitude	Longitude	Number of Intersecting Lineaments	Expansion δ (km)	Strike-Parallel O_s (km)	Morphologic Width (km)	χ^2	Resolution (m/pixel)
11	−12	145	6	2.88 ± 1.10	0.82 ± 0.52	4–5	1.78	211.26
1.1	41	−150	5	8.61 ± 0.85	4.09 ± 0.30	11–24	3.28	169.37
12.2	8	140	6	2.10 ± 0.49	4.33 ± 0.36	6–8	0.15	226.00
13	23.5	137	15	0.94 ± 0.35	0.98 ± 0.16	3–6	0.58	227.99
14	15	86	12	2.19 ± 0.37	−1.99 ± 0.13	6–9	4.19	182.50
12.1	5	135	11	3.28 ± 0.38	1.38 ± 0.26	6–7	0.95	226.00

[a]Same format as Table 1, with the addition of width range. The error on each of the measured widths is ±0.5 km.

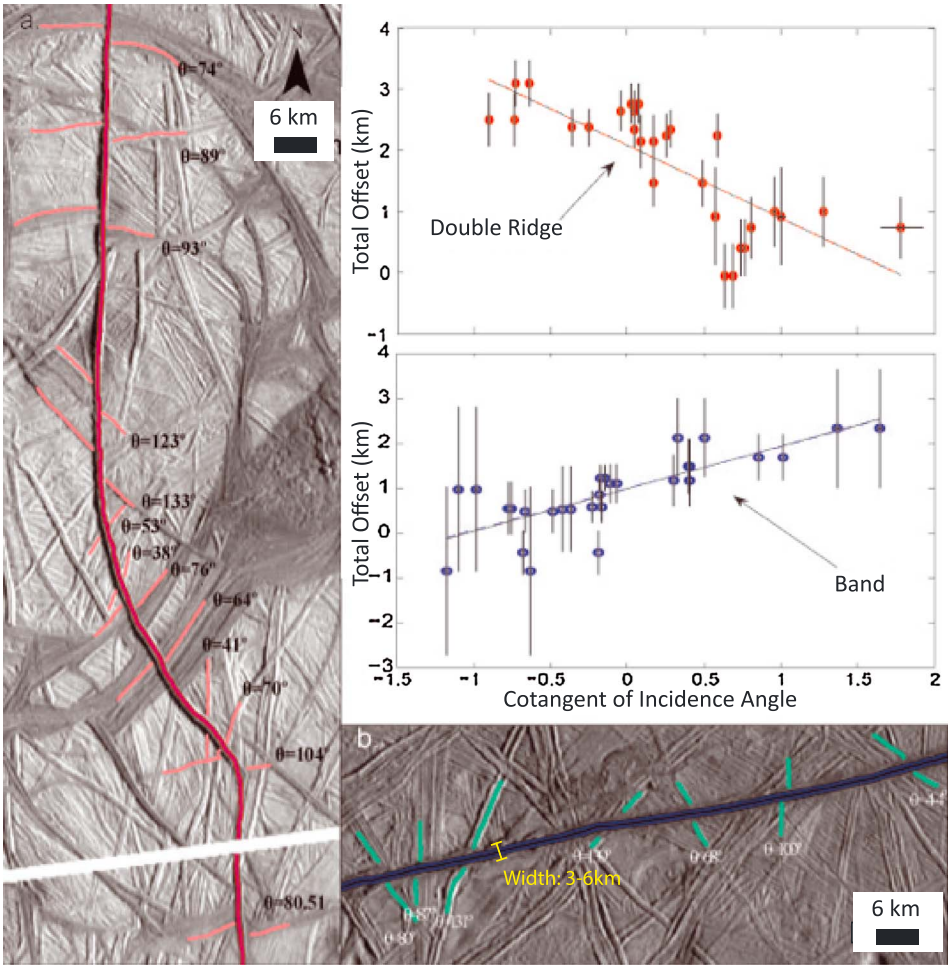

Figure 4. (a) Double ridge at −15°N and 140°E (region 2) that records contraction, $\delta = -1.19 \pm 0.15$ km, and right-lateral strike-slip displacement, $O_s = 2.08 \pm 0.08$ km. (b) Band at 22°N and 130°E (region 13) that records dilation, $\delta = 0.94 \pm 0.35$ km and right-lateral strike-slip motion $O_s = 0.98 \pm 0.16$ km. The morphologic width for this band varies between 3 and 6 km. This band was also analyzed by *Coulter* [2009], who obtained similar results. Inset shows the relationship between offset and incidence angle for each feature. The entire region that is mapped is not shown in the figure.

the strike-parallel component varies between -0.84 ± 0.23 km (left lateral) and 1.00 ± 0.13 km (right-lateral). The expanded features show a variety of strike-parallel motions.

Of all 16 double ridges, four are ambiguous such that the uncertainty is too high to state if it has contracted or expanded to within a 68% confidence limit (1 standard deviation). This is true for one of the double ridges that shows contraction and three of the double ridges that show expansion. There are more uncertain cases for expanded double ridges.

Figure 5 compares the relationship between strike-perpendicular motion and strike-parallel motion. For double ridges, there is a rough linear correlation between strike-parallel and strike-perpendicular displacement, with a Pearson correlation coefficient of $R = -0.6$: features with larger magnitude of contraction are associated with large amounts of right-lateral strike slip. The relation can be described by

$$(-0.8 \pm 0.2) \cdot \delta + (0.3 \pm 0.6) = O_S \quad (2)$$

where δ is strike-perpendicular motion and O_S is strike-parallel displacement.

3.2. Bands

Figure 4b shows an expanded band with $\delta = 0.94 \pm 0.35$ km, $O_S = 0.98 \pm 0.16$ km, and a width that varies between 3 and 6 km.

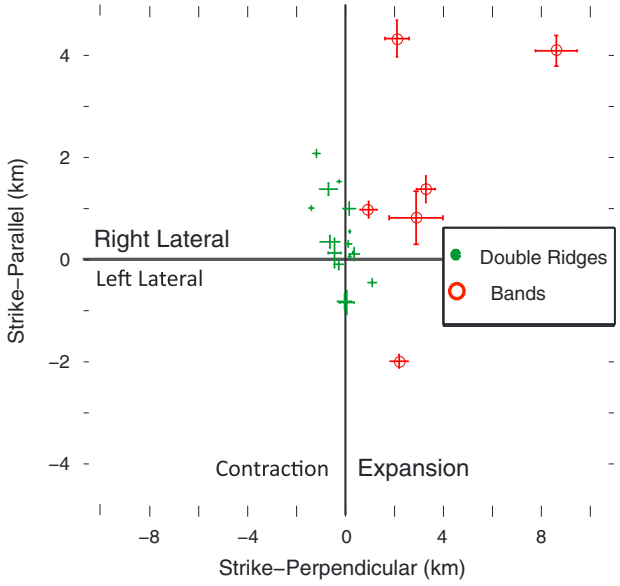

Figure 5. Strike-parallel and strike-perpendicular displacements for all 22 mapped features. The red open circles are bands and green dots are double ridges.

Of the bands, five record right-lateral motion (up to 4.33 ± 0.36 km of offset) and one shows left-lateral motion (−1.99 ± 0.13 km). All of the bands involve a component of expansion (between 0.94 ± 0.35 and 8.61 ± 0.85 km). Our results also show that the morphologic width is larger than the measured expansion (Table 1). Our results confirm previous studies that show that common bands are formed by expansion and strike-parallel motion [*Head and Pappalardo*, 1999; *Prockter et al*., 2002; *Manga and Sinton*, 2004; *Aydin*, 2006].

The main differences between ridges and bands are as follows. Bands record expansion compared to double ridges, which preserve contraction and expansion. The magnitude of perpendicular displacement, $|\delta|$, is much larger for bands than for ridges. Bands do not show a relation between strike-perpendicular and strike-parallel motion, as ridges do (Figure 5).

4. Discussion

One puzzling aspect of the tectonic features on the surface of Europa is the paucity of features that record contraction to balance the expansion produced by bands. Changes in volume of Europa from time variations in the thickness and temperature of the ice shell [*Hussmann and Spohn*, 2004; *Mitri and Showman*, 2005] are at least an order of magnitude too small to account for the observed extension [*Nimmo*, 2004; *Manga and Wang*, 2007], but changes in porosity could explain the lack of visible evidence for compression [*Pappalardo and Davies*, 2004]. Observational evidence for contraction is preserved in folds with small amplitudes [*Prockter and Pappalardo*, 2000] though these folds do not record enough strain to accommodate the expansion elsewhere [*Dombard and McKinnon*, 2006]. There are also no large-amplitude folds with smaller strains [*Bland and McKinnon*, 2012]. Bands [*Greenberg*, 2004], strike-parallel faults [*Sarid et al*., 2002], and ridges [*Patterson and Pappalardo*, 2002] have been proposed as sites of convergence, though quantification of the magnitude has been limited.

We have documented here that double ridges can preserve contraction, which is evident in their crosscutting relationships. In order to assess the amount of strain that ridges might accommodate, we assume that the ridges and bands remain intact, enabling us to make some extrapolations. The average spacing is estimated by identifying the number of double ridges that intersect a given line on the surface (Figure 1c). Multiple locations were chosen and scaled by their resolution. Over a total length of 12,501 km, we count 1,735 double ridges. Assuming that these values are representative of the entire surface, ridges are spaced 7.2 ± 3.5 km apart. The mean fault-perpendicular displacement for all 16 double ridges (including ridges with expansion or ambiguity) is 0.16 ± 0.06 km (net contraction). The observed net contraction is supported by the dominance of double ridges on the contraction half of the plot. The implied mean strain is 2.2 ± 0.8%. This value is compatible with the analysis of *Patterson et al*. [2006], who found a ~1% surface loss in the region around ~230° longitude and ~0° latitude.

We measure a mean spacing of bands of 43.8 ± 15.7 km, using the same approach we used to measure the spacing of ridges. The mean fault-perpendicular displacement for six bands is 3.3 ± 0.3 km. However, this is a small fraction of the satellite's surface (we observe less than 1% of the visible features), and there are numerous types of bands that might have experienced varying deformation. Our study is versatile enough to include most types of bands, but we do not include some such as gray bands [*Kattenhorn and Hurford*, 2009;

Prockter and Patterson, 2009] and wide bands (e.g., Libya Linea and Thynia Linea). Different types of bands might form through different mechanisms, at different rates, or from different materials [*Hoyer et al*., 2013; *Prockter and Pappalardo*, 2000; *Greeley et al*., 1998; *Marshall and Kattenhorn*, 2005]. Nevertheless, if generalized, our results imply a mean strain of 7.6 ± 3.7%, *Figueredo and Greeley* [2004] conducted pole-to-pole mapping of all features on Europa between 80°W and 220°W longitude. While they do not report a value for the band strain or the fractional area covered by bands, our analysis of their mapping results indicates that ~15% of Europa's total surface area is covered by bands (including all band classifications). We obtain this number by averaging the percent surface area covered by bands that they documented for each latitudinal range, excluding polar regions to minimize optical errors [*Figueredo and Greeley*, 2004; P. Figueredo, Arizona State University, unpublished dissertation, 2002]. A value of 15% is greater than the mean strain we calculated and consistent with our observation that band morphologic widths are greater than the expansion preserved by crosscutting geometries (Table 2).

One of the objectives of mapping displacements perpendicular to ridges is to gain insight into how they form and to evaluate some of the proposed formation mechanisms. We recognize that double ridges can show contraction and expansion, but more double ridges show contraction within error. Most models predict extension, either from flow created by rising diapirs [*Head and Pappalardo*, 1999], cryovolcanic eruptions [*Fagents*, 2003], or tidal pumping of water through fissures to the surface [*Greenberg et al*., 2000]. Models that involve strike-parallel displacements [e.g., *Nimmo and Gaidos*, 2002] may lead to contraction: *Nimmo and Gaidos* [2002] hypothesize that any melt water generated along the shear zone may cause contraction as the melt drains downward. Although ridges produced by folding [*Manga and Sinton*, 2004] would involve contraction, the spatial resolution of our mapping is insufficient to distinguish between distributed contraction, the product of folding, and contraction along a line at the center of the ridge. None of the proposed models clearly account for both the compressional and extensional motion we observe for double ridges.

We also observe a correlation between strike-parallel and strike-perpendicular motion (Figure 5), with 0.8 ± 0.2 km of ridge-normal displacement for every kilometer of strike-parallel displacement. While we have been able to map only a limited number of features, hence the relationship shown in Figure 5 may not hold globally, the correlation implies a consistent strain along ridges. The origin and implications, either for the forces driving the formation of ridges or the mechanisms that create ridges, remain unclear but may be worthy of further study.

For the studied regions, our results show that bands preserve net expansion while double ridges preserve net contraction, suggesting that double ridges may accommodate some of the expansion associated with band formation. All of the observed bands show expansion less than their morphologic width. There are two proposed end-member conceptual models for bands, a fast-spreading limit in which the band is composed entirely of new crust, and a slow-spreading case in which displacements along dipping faults accommodate some of the extension [*Prockter et al*., 2002]. Since the width of the band exceeds the extension we measure, our data favor the slow-spreading model. The surface morphology produced by sets of dipping perpendicular faults may allow resurfacing by cryovolcanism, creating new surface area that could exceed the actual tectonic extension [*Patterson and Head*, 2003]. Repeated folding and resurfacing is another possible model and allows the width of the feature to exceed the amount of extension [*Manga and Sinton*, 2004]. Models in which bands are generated by strike-parallel motion [*Schulson*, 2002] or through cyclical tension [*Greenberg et al*., 1998] do not explain why bands appear to be wider than the measured dilation.

5. Summary

By analyzing crosscutting relationships along lineaments, we are able to identify displacements both along strike and perpendicular to the lineament. We provide quantitative demonstration of contraction using an independent method and a larger sample size when compared to previous work addressing contraction. We confirm that double ridges can record contraction [*Patterson et al*., 2006]. We also confirm that bands show expansion, but the recorded expansion along strike is less than the morphologic width. Upscaling to a global estimate of contraction across ridges, we suggest that the expansion recorded by bands may be partly accommodated by contraction about ridges. These measurements provide constraints for models for the formation of bands and double ridges. The reliability of the global extrapolation, however, is limited by the small fraction of surface images at high resolution. Global, high-resolution images better than ~ 20 m/pixel will overcome this limitation.

Acknowledgments
We thank the two reviewers, Patricio Figueredo, Guiseppe Mitri, Alyssa Rhoden, and Terry Hurford for discussions and suggestions. Culha received support from the Ramsden Foundation and National Science Foundation. Hayes acknowledges the Miller Institute for Basic Research in Science for partly funding his contributions. Thomas was partially supported by a National Science Foundation postdoctoral fellowship. We all thank NASA and NSF for making this research possible.

References

Aydin, A. (2006), Failure modes of the lineaments on Jupiter's moon, Europa: Implications for the evolution of its icy crust, *J. Struct. Geol.*, *28*, 2222–2236, doi:10.1016/j.jsg.2006.08.003.

Bland, M. T., and W. B. McKinnon (2012), Forming Europa's folds: Strain requirements for the production of large-amplitude deformation, *Icarus*, *221*, 694–709, doi:10.1016/j.icarus.2012.08.029.

Coulter, C. E. (2009), Kinematic and morphological evolution of Europa's ridges, MS thesis, Dept. of Geology, Univ. of Idaho, Moscow, Idaho.

Dombard, A. J., and W. B. McKinnon (2006), Folding of Europa's icy lithosphere: An analysis of viscous-plastic bulking and subsequent topographic relaxation, *J. Struct. Geol.*, *28*(12), 2259–2269, doi:10.1016/j.jsg.2005.12.003.

Fagents, S. A. (2003), Considerations for effusive cryovolcanism on Europa: The post-Galileo perspective, *J. Geophys. Res.*, *108*(E12), 5139, doi:10.1029/2003JE002128.

Figueredo, P. H., and R. Greeley (2004), Resurfacing history of Europa from pole-to-pole geological mapping, *Icarus*, *167*, 282–292, doi:10.1016/j.icarus.2003.09.016 .

Greeley, R., et al. (1998), Europa: Initial Galileo observations, *Icarus*, *135*, 4–24.

Greeley, R., et al. (2000), Geologic mapping of Europa, *J. Geophys. Res.*, *105*, 22,559–22,578.

Greenberg, R. (2004), The evil twin of Agenor: Tectonic convergence on Europa, *Icarus*, *167*(2), 313–319, doi:10.1016/j.icarus.2003.09.025.

Greenberg, R., et al. (1998), Tectonic processes on Europa: Tidal stresses, mechanical response, and visible features, *Icarus*, *135*, 64–78, doi:10.1006/icar.1998.5986.

Greenberg, R., P. Geissler, B. R. Tufts, and G. V. Hoppa (2000), Habitability of Europa's crust: The role of tidal-tectonic processes, *J. Geophys. Res.*, *105*(E7), 17,551–17,562, doi:10.1029/1999JE001147.

Head, J. W., and R. T. Pappalardo (1999), Brine mobilization during lithospheric heating on Europa: Implications for formation of chaos terrain lenticular texture, and color variations, *J. Geophys. Res.*, *104*, 27,143–27,155, doi:10.1029/1999JE001062.

Hoppa, G. V., B. R. Tufts, R. Greenberg, and P. Geissler (1999), Strike-slip faults on Europa: Global shear patterns driven by tidal stress, *Icarus*, *141*, 287–298.

Hoyer, L., S. A. Kattenhorn, and M. K. Watkeys (2013), Multistage evolution and variable motion history of Agenor Linea, Europa, *Icarus*, *1016* 390–402, doi:10.1016/j.icarus.2013.12.010.

Hussmann, H., and T. Spohn (2004), Thermal-orbital evolution of Europa, *Icarus*, *171*, 391–410, doi:10.1016/j.icarus.2004.05.020.

Kadel, S., S. A. Fagents, R. Greeley, and The Galileo solid-state imaging team (1998), Trough-bounding ridge pairs on Europa consideration for an endogenic model of formation, Lunar and Planetary Science Conference, abstract #1078.

Kattenhorn, S. A., and T. A. Hurford (2009), Tectonics of Europa, in *Europa*, edited by R. T. Pappalardo, W. B. McKinnon, and K. Khurana, pp. 199–236, Univ. of Ariz. Press.

Manga, M., and A. Sinton (2004), Formation of bands and ridges on Europa by cyclic deformation: Insights from analogue wax experiments, *J. Geophys. Res.*, *109*, E09001, doi:10.1029/2004JE002249.

Manga, M., and C.-Y. Wang (2007), Pressurized oceans and the eruption of liquid water on Europa and Enceladus, *Geophys. Res. Lett.*, *34*, L07202, doi:10.1029/2007GL029297.

Marshall, S. T., and S. A. Kattenhorn (2005), A revised model for cycloid growth mechanics on Europa: Evidence from surface morphologies and geometries, *Icarus*, *177*, 341–366.

Mitri, G., and A. P. Showman (2005), Convective-conductive transitions and sensitivity of a convecting ice shell to perturbations in heat flux and tidal-heating rate: Implications for Europa, *Icarus*, *177*, 447–460.

Nimmo, F. (2004), Stresses generated in cooling viscoelastic ice shells: Application to Europa, *J. Geophys. Res.*, *109*, E12001, doi:10.1029/2004JE002347.

Nimmo, F., and E. Gaidos (2002), Strike-slip motion and double ridge formation on Europa, *J. Geophys. Res.*, *107*(E4), 5021, doi:10.1029/2000JE001476.

Nimmo, F., and P. Schenk (2006), Normal faulting on Europa: Implications for ice shell properties, *J. Struct. Geol.*, *28*, 2194–2203.

Nimmo, F., R. T. Pappalardo, and B. Giese (2003), On the origins of band topography, Europa, *Icarus*, *166*, 21–32.

Pappalardo, R. T., and R. J. Sullivan (1996), Evidence for separation across a gray band on Europa, *Icarus*, *123*, 557–567, doi:10.1006/icar.1996.0178.

Pappalardo, R. T., and D. M. Davies (2004), Where's the compression? Explaining the lack of contractional structures on icy satellites, in *Workshop on Ices, Oceans, and Fire: Satellites of the Outer Solar System*, LPI Contribution No. 1357, pp. 108–109, Lunar and Planetary Institute, Houston.

Patterson, G. W., and R. T. Pappalardo (2002), Compression across ridges on Europa, in *Workshop on Ices, Oceans, and Fire: Satellites of the Outer Solar System*, LPI Contribution No. 1357, pp. 110–111, Lunar and Planetary Institute, Houston, Tex.

Patterson, G. W., J. W. Head, and R. T. Pappalardo (2006), Plate motion on Europa and nonrigid behavior of the icy lithosphere: The Castalia Macula region, *J. Struct. Geol.*, *28*(12), 2237–2258, doi:10.1016/j.jsg.2006.03.032.

Patterson, G. W., and J. W. Head (2003), Crustal spreading on Europa: Inferring tectonic history from triple junction analysis, 34th Annual LPSC, 34, 1262.

Prockter, L., and G. W. Patterson (2009), Morphology and evolution of Europa's ridges and bands, in *Europa*, edited by R. Pappalardo, W. McKinnon, and K. Khurana, pp. 237–258, Univ. of Ariz. Press, Tucson, Ariz.

Prockter, L. M., and R. T. Pappalardo (2000), Strike-slip deplexing on Jupiter's icy moon Europa, *J. Geophys. Res.*, *105*(E4), 9483–9488, doi:10.1029/19999JE001226.

Prockter, L. M., J. W. Head III, R. T. Pappalardo, R. J. Sullivan, A. E. Clifton, B. Giese, R. Wagner, and G. Neukum (2002), Morphology of Europan bands at high resolution: A mid-ocean ridge-type rift mechanism, *J. Geophys. Res.*, *107*(E5), 5028, doi:10.1029/2000JE001458.

Rhoden, A. R., G. Wurman, E. M. Huff, M. Manga, and T. A. Hurford (2012), Shell tectonics: A mechanical model for strike-slip displacement on Europa, *Icarus*, *218*(1), 297–307, doi:10.1016/j.icarus.2011.12.015.

Sarid, A. R., R. Greenberg, G. V. Hoppa, T. A. Hurford, B. R. Tufts, and P. Geissler (2002), Polar wander and surface convergence of Europa's ice shell: Evidence from a survey of strike-slip displacement, *Icarus*, *158*, 24–41, doi:10.1006/icar.2002.6873.

Schenk, P. M., and W. B. McKinnon (1989), Fault offset and lateral crustal movement on Europa: Evidence for a mobile ice shell, *Icarus*, *79*, 75–100, doi:10.1016/0019-1035(89)90109-7.

Schulson, E. M. (2002), On the origin of a wedge crack within the icy crust of Europa, *J. Geophys. Res.*, *107*(E11), 5107, doi:10.1029/2001JE001586.

Smith, A. F. M., and G. O. Robert (1993), Bayesian computation via the Gibbs sampler and related Markov chain methods, *J. Roy. Stat. Soc.*, *55*(1), 3–23.

Sullivan, R. J., et al. (1998), Episodic plate separation and fracture infill on the surface of Europa, *Nature*, 371–373, doi:10.1006/icar.1998.5969.

Tufts, B. R., R. Greenberg, G. Hoppa, and P. Geissler (2000), Lithospheric dilation on Europa, *Icarus*, *146*, 75–97, doi:10.1006/icar.2000.6369.